Available online at www.sciencedirect.com

ScienceDirect

Procedia Manufacturing 10 (2017) 497 – 509

Procedia MANUFACTURING

45th SME North American Manufacturing Research Conference, NAMRC 45, LA, USA

# Micro-milling machinability of DED additive titanium Ti-6Al-4V

Giuseppe Bonaiti[1], Paolo Parenti[1]*, Massimiliano Annoni[1], Shiv Kapoor[2]

[1]*Department of Mechanical Engineering, Politecnico di Milan, Italy*
[2]*Department of Mechanical Engineering, Univeristy of Illinois at Urbana-Champaign, USA*

**Abstract**

This work investigates the micro-milling machinability of Ti-6Al-4V alloy produced by a Laser Engineered Net Shaping (LENS) additive manufacturing (AM) process with a specific focus on surface quality, cutting forces and burr formation. The effects of additive deposition parameters are also investigated since the material thermal history during processing can affect porosity and mechanical behavior of the samples, giving different milling performances. The material characterization of samples is done through micrographies, hardness tests and porosity evaluation. The roughness of the machined surfaces shows a statistical distinction between the AM and wrought titanium samples. Similar behavior is seen with the cutting forces, which increase with an increase of hardness of the AM samples. The results also show an increased trend towards burr formation in case of down milling of AM samples compared to wrought titanium samples. The future prospective is to take into account the machinability properties as functional material characteristics to optimize through the deposition process.


Peer-review under responsibility of the organizing committee of the 45th SME North American Manufacturing Research Conference

*Keywords:* Machinability; Titanium alloys; Micro-milling; Additive manufacturing; Laser Engineered Net Shaping;

## 1. Introduction

The Additive Manufacturing (AM) has shown a great potential to create complex parts, starting from the addition of metal powder layer by layer and melting it by a heat source, such as a laser or an electron beam. Additive

* Corresponding author.
*E-mail address:* paolo.parenti@polimi.it


Peer-review under responsibility of the organizing committee of the 45th SME North American Manufacturing Research Conference
doi:10.1016/j.promfg.2017.07.104

Manufacturing techniques can be classified in two main categories: (1) powder bed techniques, such as Direct Metal Laser Sintering (DMLS) and (2) blown powder techniques, such as Laser Engineered Net Shaping (LENS) / Direct Energy Deposition (DED). In particular, the LENS additive manufacturing technology was first developed by Sandia National Laboratories in the late 1990s [1]. The added value of this AM technology is the ability to produce and clad complex metallic geometries that are difficult to manufacture through conventional metal forming techniques and the capacity to provide increased mechanical properties of the components. However, the current AM processes available in industry are not able to achieve tight geometrical tolerances and good surface roughness and therefore, post-processing operations including grinding, milling, abrasive flow machining are usually required [2,3]. The milling process is shown to offer the best solution to finish external geometries for a wide variety of materials with reasonable surface quality. Several research studies have been performed to study the machinability of titanium alloys for several industrial applications [4-7]. The main problems of Ti-6Al-4V are related to its high strain-hardening behavior, chemical reactivity and low thermal conductivity, which accelerate tool wear. When scaling down the tool dimensions to micro-milling cases, these aspects worsen and this difficult-to-cut material requires specific cutting conditions [8-9]. On the other side, machinability of additive manufacturing metals is still not well understood and only very few and recent literature studies exist. Very recently, Guo et al. [10] focused their study on additive manufactured AISI 316L, whilst Montevecchi et al. [11] carried out cutting tests on wrought, LENS and WAAM (WireArc AM) processed AISI H13 samples, by analysing the subsequent cutting forces. The results highlight that AM materials are harder to machine as compared to the wrought state and show a significant increase in cutting forces. Machinability of AM Titanium and its alloys is even less explored. Tebaldo and Faga [12] studied the heat treatment effects on Ti48Al2Nb2Cr AM titanium obtained by electron beam melting, finding that the induced microstructural changes play a major role on the machinability. At the same time, Bruschi et al. [13] and Rysava et al. [14] recently studied micro-milling, micro-drilling and threading of titanium alloys produced by AM processes, finding that a proper selection of cutting process conditions is a key phase for achieving good machining results.

At the same time, there have been many research works about the characterization of mechanical properties of various types of titanium alloys manufactured by AM processes [15,16]. In particular, Kbryn et al. [15] studied the effect of process parameters including laser power and traverse speed on microstructure, porosity and texture of Ti-6Al-4V. The AM components were found to possess a columnar microstructure and a fine Widmanstätten microstructure. Their work also demonstrated that an increase in the laser power and traverse speed causes a decrease in porosity in terms of lack-of-fusion and gas entrapment.

The purpose of this research is to study the machinability of LENS AM Ti-6Al-4V by conducting micro end milling tests. Specifically, the machinability is evaluated by comparing LENS AM Ti-6Al-4V with wrought titanium in terms of roughness, cutting force and burr formation. The description of machines and materials, including material sample preparation and material characterization (micrography, porosity and hardness evaluation) is reported in Section 2 while the experimental work is detailed in Section 3. Results and machinability analyses are given in Section 4. Finally, the conclusions drawn from this work are presented in Section 5.

## 2. Machines and Materials

### *2.1. Machine*

The micro-end milling operation for the roughness analysis are carried out on Microlution 310-S, the 3-axis micro-milling machine, which is capable of spindle speeds up to 50,000 rpm, 1 µm positioning accuracy, 0.02 µm resolution and a maximum acceleration of 5 g. Meanwhile, the cutting force and burr formation analysis are carried out on a 5-axis Kern EVO CNC machining center equipped with a Heidenhain iTNC530 numerical control (1 µm positioning accuracy).

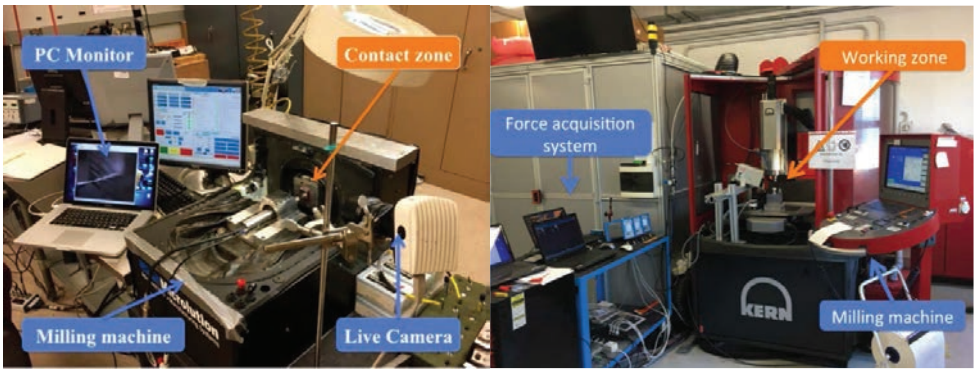


Figure 1: Equipment: Microlution310-S (left), Kern EVO (right)

### *2.2. LENS AM Ti-6Al-4V*

Three Ti-6Al-4V cubic components were built with the LENS technology. The used Sandia Optomec LENS system is characterized by 1 kW Ytterbium continuous wave (CW) fiber optic laser with a Gaussian beam, inert gas operations, 4-axis capability and 300 mm x 300 mm x 300 mm working volume. The Ti-6Al-4V powder size distribution was between 45 and 106 µm. The material chemical composition is detailed in Table 1 [17].

Table 1: Chemical analysis

| | **Ti** | **Al** | **V** | **Fe** | **$0_2$** | **$N_2$** | **C** | **Other** |
|---|---|---|---|---|---|---|---|---|
| % | Bal. | 6.35 | 4.0 | 0.21 | 0.06 | 0.02 | 0.01 | < 0.40 |

The three Ti-6Al-4V cubic components had dimensions of 40 mm x 40 mm x 40 mm and were built on an unheated substrate plate of the same material within the LENS system. The cubic components were built with the same tool path and process parameters, apart from the input laser processing power. The laser beam had a diameter of 1.83 mm and was set at three power levels (710 W – 800 W – 940 W). A built-in algorithm for parameters selection indicated 800 W as the optimal power. The other two levels were adjusted for this study (Table 2). The layer thickness and hatch spacing were set at 0.95 mm and 1.20 mm, respectively.

Table 2: LENS deposition process parameters

| **Process parameters** | **Additive A** | **Additive B** | **Additive C** |
|---|---|---|---|
| Output laser power | 710 W | 800 W | 940 W |
| Travel speed | 10 mm/s | 10 mm/s | 10 mm/s |
| Powder feed rate | 0.12 g/s | 0.12 g/s | 0.12 g/s |

Since the original dimensions of the AM samples were too big and the specimens too heavy to install directly on the micro-machine, it was decided to cut them into slices of 3 mm in thickness. A particular attention was paid to the cutting procedure, since it could alter the microstructure of the samples. In order to limit the microstructure alterations, a wire EDM machine (Charmilles Robofil 290 F) was used to cut the AM material.

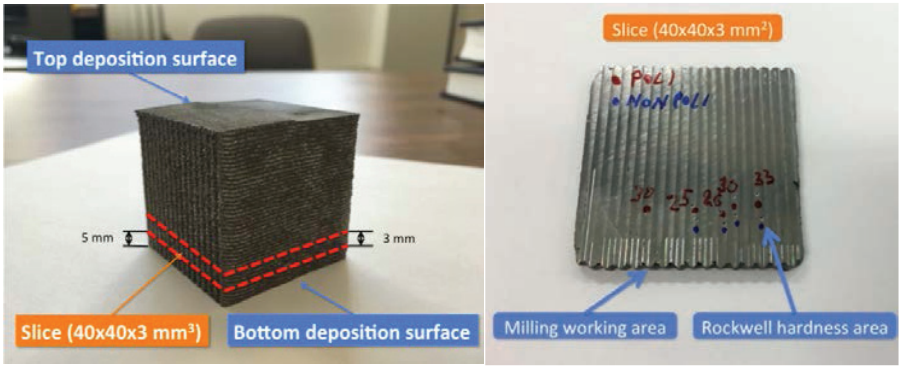


Figure 2: Specimen preparation, milling working area and hardness measurement points.

### *2.3. Material characterization*

The primary alloying elements in Ti-6Al-4V are aluminum (Al), vanadium (V) with traces of oxygen (O) and nitrogen (N). The behavior of the Ti-6Al-4V alloy that could affect its machinability is strongly influenced by the process parameters and thermal history of the applied manufacturing processes. In this section, the material characterization of AM Ti-6Al-4V is carried out in terms of microstructural, hardness and porosity analysis. The porosity evaluation is helpful for selecting a surface unaffected by pores to machine.

#### *Micrography*

For the microstructural examination of wrought and AM Ti-6Al-4V, samples were sectioned using a silicon carbide cutting blade at a low cutting speed of 0.2 mm/min with ample amount of water based coolant. The samples were then mounted on a support and were then mechanically polished using 220, 400, 600, 800 and 1200 silicon carbide grit papers. After plane grinding with grit paper, final polishing was done. Kroll's reagent, consisting of 3 ml of HF, 6 ml of $HNO_3$ and 100 ml of distilled water, was used as an etchant. The specimens were etched for 30 s in the Kroll's reagent at first and then again for about 2 minutes.

The micrographies of four materials are shown in Figure 3. The microstructure of the three LENS samples (Additive A, B and C) presents the typical martensitic structure expected for the Ti-6Al-4V alloy, rapidly cooled from the beta-phase field [18]. For the standard wrought Ti–6Al–4V titanium, the micrography revealed a duplex microstructure consisting of the near equiaxed alpha (α) and transformed beta (β) phases. The α grains (light) are well distributed and the transformed β (dark phase) are present at the boundary of the grains. It is also clear from Figure 3 that the alpha (α) grains are somewhat elongated in the rolling direction.

#### *Hardness*

It has been reported in literature [19] that the AM parts hardness tends to vary significantly from top and bottom layers to the middle layer of the part, since the cooling rate of the melt pool and velocity of solidification are slower in the middle region than in the top and bottom regions. Further, the middle region is exposed to cyclic reheating from the deposition of subsequent layers. Thus, it is essential to have an estimate of sample hardness values before conducting the machinability study.

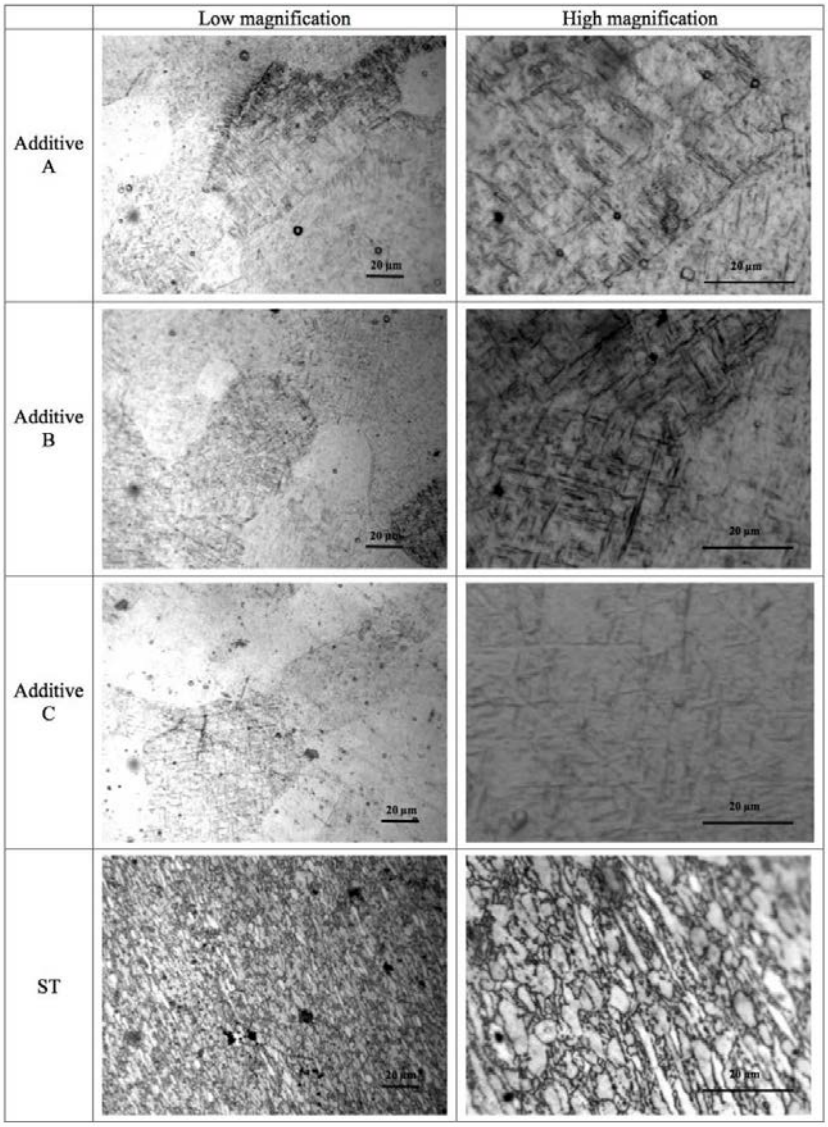


Figure 3: Additive and standard titanium micrographies

In this research, the hardness tests are performed on a Wilson Rockwell machine, following the ISO 6508-1 standard. Each time a new set of measurements is performed, a measurement with a calibrated sample is made on a hardness standard block test of 25 HRC. The hardness test is carried out three times per material. The specimens hardness results are presented in Table 3. From the results in Table 3, it is possible to see how a laser power increase can cause an increase in the Rockwell Hardness (HRC) values. The experimental results also suggest that the hardness values vary with the material microstructure.

Table 3: Tested materials hardness (HRC)

| Additive A | Additive B | Additive C | Standard |
|---|---|---|---|
| 28.0 ± 1.4 | 34.9 ± 1.5 | 37.6 ± 1.1 | 28,3 ± 0.7 |

*Porosity analysis*

The porosity analysis was done using a North Star X 25 3D computer tomography system to assess the overall porosity structure and to identify and locate the pores position and plan milling operations on unaffected areas. The AM samples scans were post-processed using the efX-ct software to construct a 3D image of the specimen. It was found that the porosities were parallel to the deposition trace of the LENS path, at the boundary of the weld beads. From the reconstructed images, two cross-sections-one with a plane parallel to the deposition layer and the other perpendicular to the deposition plan were obtained. Figure 4 shows the two cross-section images. It is seen from Figure 4 that the porosity decreases from sample A to sample B, and reduces further for sample C. These results were confirmed by conducting porosity tests using Archimedes method, where it was found that the overall porosity for sample A was 2.11% as compared to 1.62% for sample B and 0.88% for sample C, respectively. From the 3D tomography reconstructions, the exact cutting path for the following micro-milling experiments was identified in order to prevent intermittent cutting due to pores present in the samples.

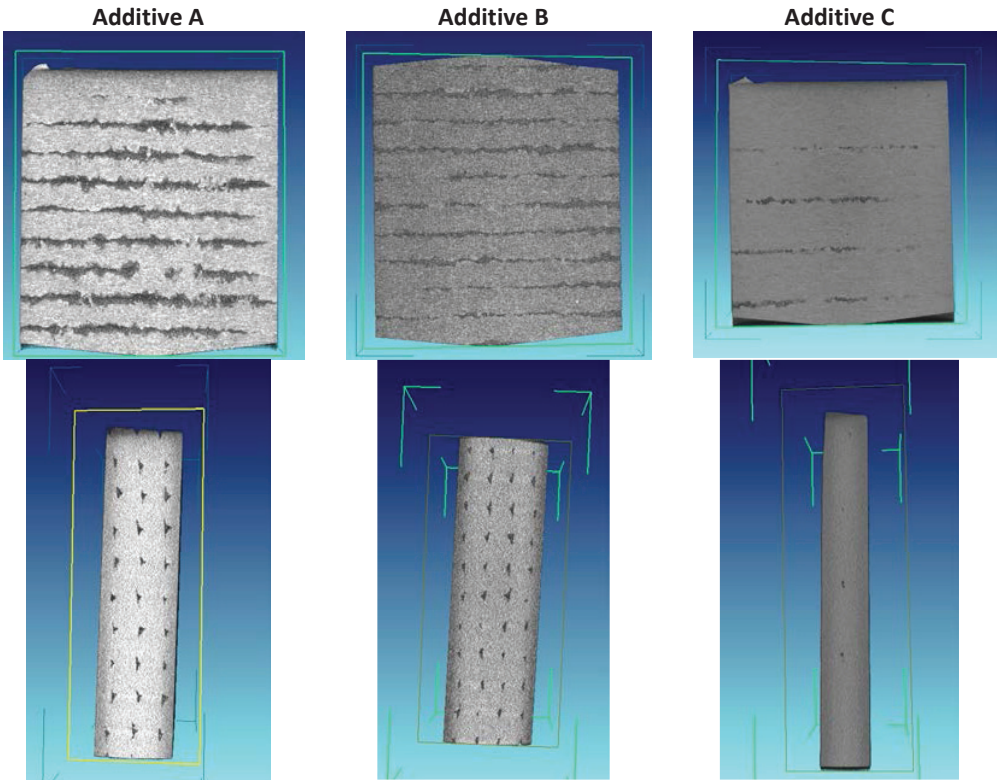


Figure 4: Parallel (first row) and perpendicular (second row) cross sections

## 3. Experiments

In this section, the details of the experimental plan to collect and analyze machinability data in terms of roughness, cutting force and burr produced by the end milling operations is presented.

### *3.1. Roughness*

A factorial Design Of Experiments (DOE) methodology was used to conduct machining tests for evaluating the surface roughness of AM samples. Four materials (Additive samples A, B and C and standard wrought titanium alloy), three levels of axial depth of cut (25/50/75 μm), and three levels of feed per tooth (2/3.5/5 μm/tooth) were employed. Each full slotting test was replicated, resulting into a total of 72 tests. The Microlution 310-S 3-axis micro-milling machine was used for the experiment. The TS-2-0200-S tools (2-flute, 508 μm – 0.02 inch, tool nominal diameter) from Performance Micro Tools were selected for end milling grooves with a cutting speed of 25.5 m/min (spindle speed = 16 krpm). Each experiment was randomized. In order to avoid machining with tool wear, a new tool was used after machining every five grooves. Figure 5 shows an SEM image of the carbide TS-2-0020-S cutting tool.

Figure 5: SEM images of the carbide TS-2-0200-S tool

Surface roughness was measured using the Dektak 3030 profilometer with stylus radius of 2.5 μm. A travel length of 1000 μm with sampling length of 800 μm was used to evaluate the surface roughness with a cut-off frequency of 800 μm (according to ISO 4287:1997). For every machined groove, measurements were made at three different locations, i.e. start, center and end as shown in Figure 6. Each measurement was repeated two (2) times and the average and standard deviation of the roughness values were computed.

### *3.2. Cutting force*

The 5-axis Kern EVO CNC machining center machine was used for the experiment. Tests were performed with two (2) variables including materials (Additive A/B/C and standard wrought titanium alloy) and feed per tooth (10/17.5/25 μm/tooth). Each test was replicated 3 times for a total number of 9 tests performed on each of the 4 material samples, resulting in a total number of 36 tests. The Mitsubishi MS2SS D0150 2-flute flat end mill was used with a cutting speed of 85 m/min (spindle speed = 18 krpm), axial depth of cut $a_p$= 100 μm, radial depth of cut $a_e$= 450 μm. The cutting forces were acquired through a Kistler 9317B piezoelectric triaxial dynamometric load cell, three Kistler 5015A charge amplifiers (one per machine Cartesian component), and an acquisition board connected to a PC with an acquisition program. The Fx, Fy, Fz forces were recorded for each of 36 tests and the total average force Fr (calculated all along the slot length) was evaluated.

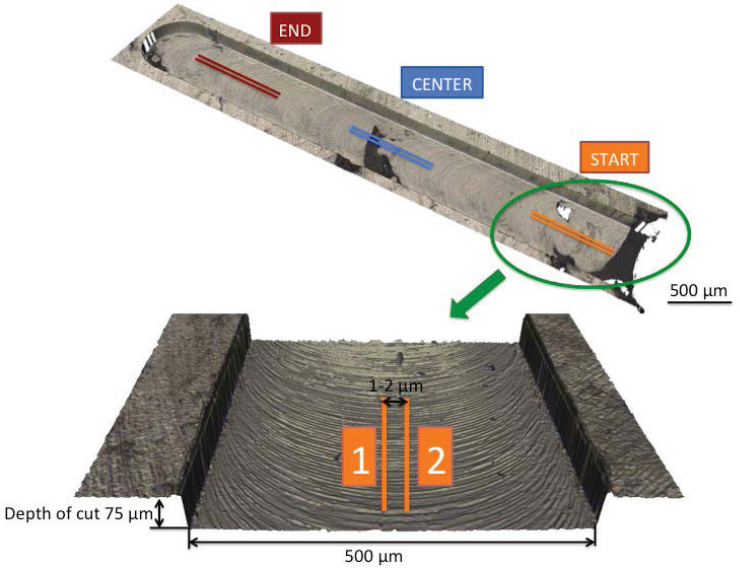


Figure 6: Cross section perpendicular to the deposition layer

### *3.3. Burr formation*

The description and the definition of machining burrs are not unique. They strongly depend on the machining process and mechanical properties of the work material. In this section, the burr is considered as an accumulation of material on the edges of a workpiece. The burrs do not necessarily occur on all edges of the workpiece. In face milling, as shown in Figure 7, eight burr locations were identified by Hashimura et al. [20]. In the present study, the top burr in position no. 10 (Figure 7) was analyzed and compared among various titanium samples. A Mitutoyo Vision Measuring System Microscope was used to observe the top burr images after machining.

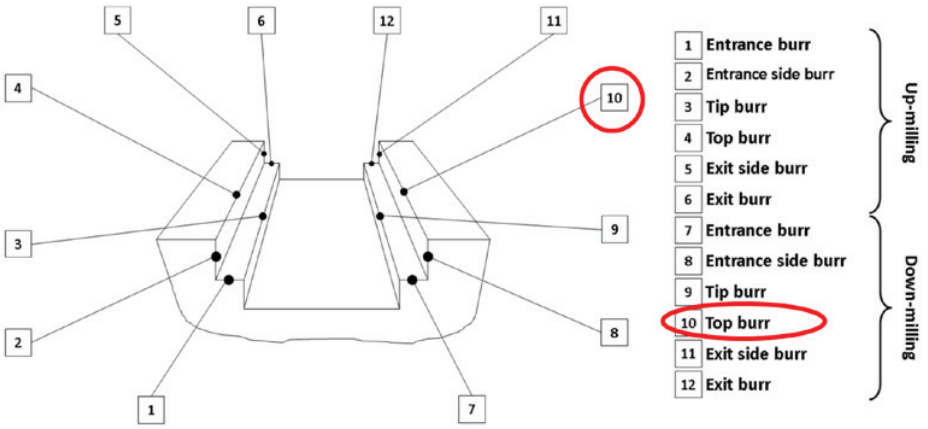


Figure 7: Hashimura burr locations [20]

## 4. Experimental results

### *4.1. Roughness*

Figure 8 shows the main effects of material, depth of cut and feed per tooth on surface roughness. The depth of cut and feed per tooth seem to have a direct positive effect. However, the effect of material type shows a specific trend. This trend presents a clear distinction from the additive materials A, B and C and the standard titanium, probably due to a different microstructure of the titanium samples.

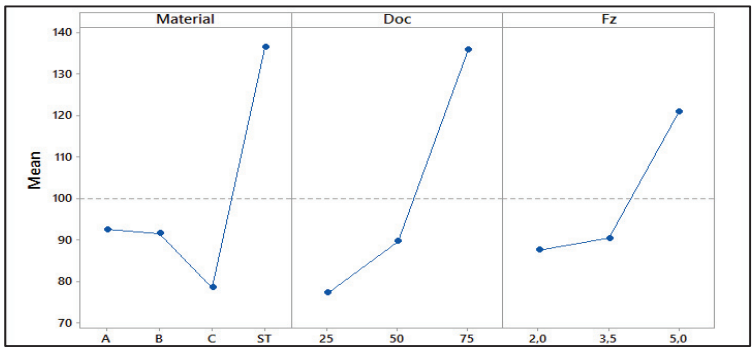


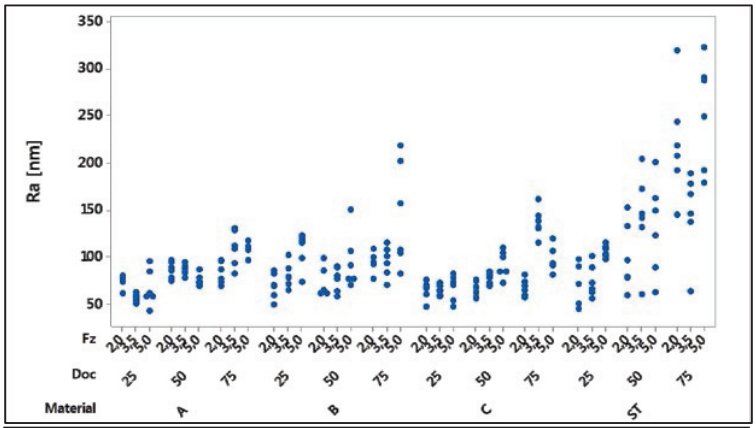


| Source | DF | Adj SS | Adj MS | F-Value | P-Value |
|---|---|---|---|---|---|
| Material | 3 | 33744 | 11247,9 | 12,80 | 0,000 |
| Doc | 2 | 41059 | 20529,3 | 23,36 | 0,000 |
| Fz | 2 | 14923 | 7461,4 | 8,49 | 0,001 |

Figure 8: Analysis of Ra: Main effect plot, Individual value plot, reduced ANOVA table

The result of the Tukey comparison (Table 4) shows a significant statistical difference among material levels. Further, it is seen from the roughness values that, on average, the standard wrought titanium has much higher roughness value than the three AM materials. In fact, the three AM material samples show similar roughness values.

Table 4: Table of Tukey Pairwise Comparisons (95% CI): Response = Ra, Term = Material

| Material | N | Mean | Grouping |
|---|---|---|---|
| ST | 18 | 136.385 | A |
| A | 16 | 95.449 | B |
| B | 18 | 91.571 | B |
| C | 18 | 78.481 | B |

### *4.2. Cutting force*

Figure 9 shows the total resultant cutting force variation for four materials and three feeds per tooth. As expected, the resultant force increases with an increase in feed per tooth. The increasing trend in forces is also seen for the type of materials machined, however, a high variation of the forces can be seen for the material C. The increasing trend could be related to the microstructure properties and hardness values. As the hardness of the additive materials increase, the total force also increase (refer to Table 3). The forces for the standard titanium material, however, are found higher than the AM materials irrespective of its lower hardness value. One possible reason could be that the microstructure of the standard titanium sample consists of equiaxed alpha (α) and transformed beta (β) phases with some elongated grains that could create resistance to the cutting action.

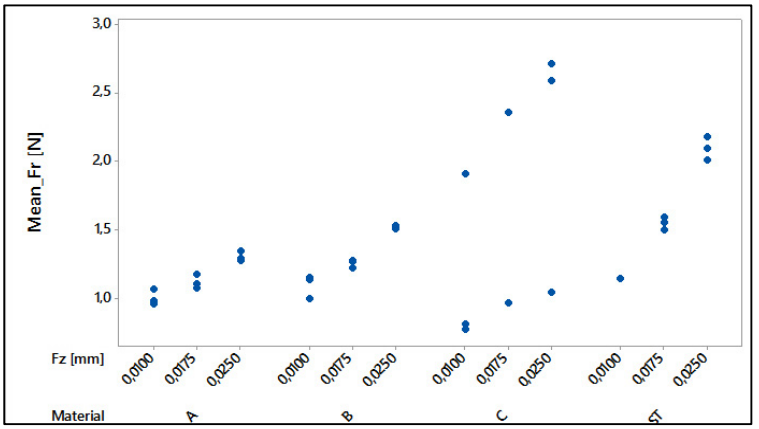


Figure 9: Total average resultant force Fr

### *4.3. Burr formation results*

The full slot milling operations are conducted on four material samples and the top burr on the down milling side are identified as the most relevant burr formation area. Figure 10 shows the top burr images for one of the cutting tests defined earlier in Section 3.2. It is seen from Figure 10 that there are little or no burrs formed when machining the standard titanium material sample. However, significant burrs are observed for the AM material samples. In fact, the top burr increases significantly from sample A to sample C. This increase could very well be related to the hardness of the samples or the use of increased laser power during the additive manufacturing process.

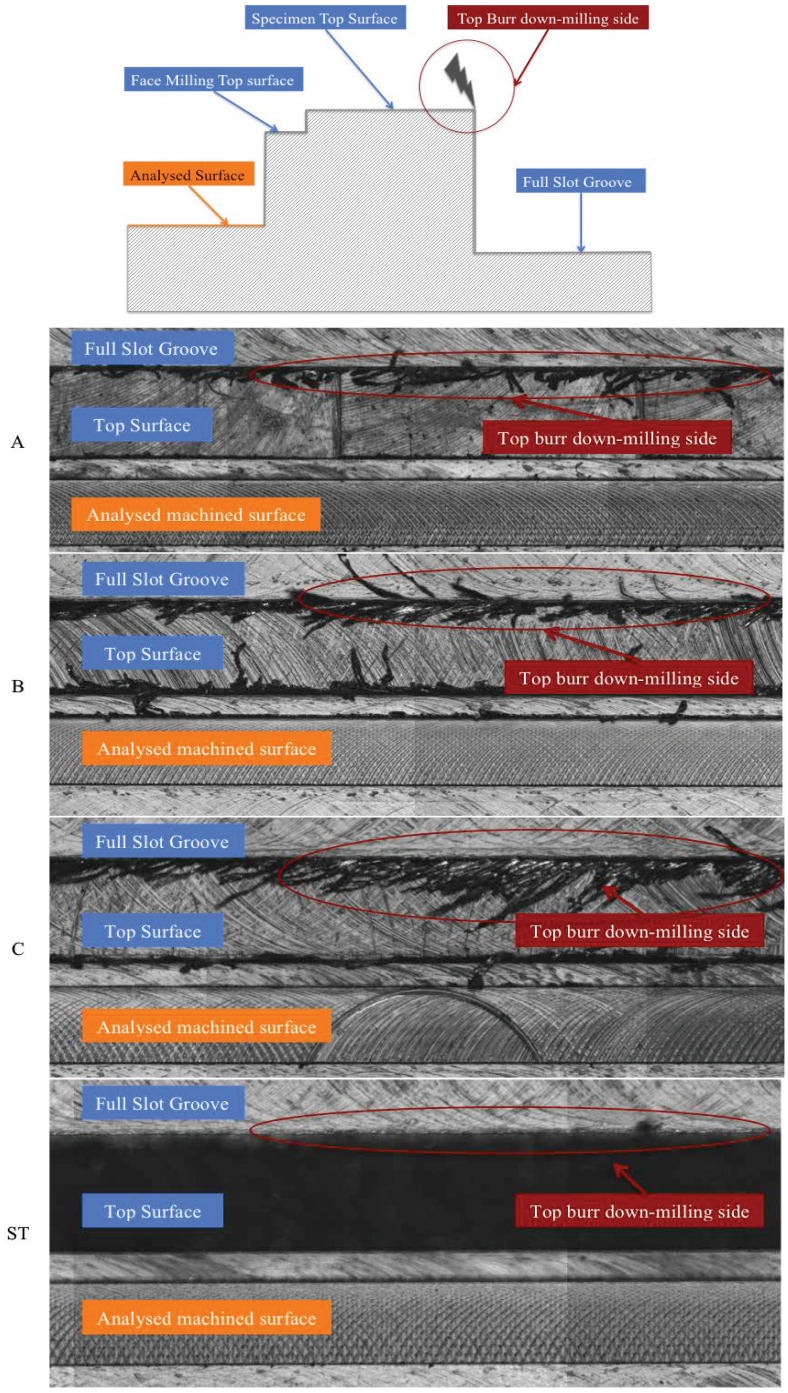


Figure 10: Burr formation: Cross-section (scheme) and Top view (microscope image)

## 5. Conclusions

This work conducted a machinability study on micro-milled additive manufactured Ti-6Al-4V samples. The microstructure analysis, hardness testing and porosity evaluation were done for material characterization. Micro-cutting tests were performed on four materials that included three materials produced by the LENS additive manufacturing process with varying laser power and one standard titanium material. Following conclusions are drawn from this study.

1. An increased hardness of AM materials is related to finer material microstructure, i.e. a finer martensite, and use of the increased laser power. The increase in laser power, however, produces lower porosity, thus improving the overall integrity of the material samples.
2. Roughness increases with the increase in cutting parameters including depth of cut and feedrate. However, an increase in hardness of AM materials produces a lower roughness value. The machining of standard titanium material produces a much rougher surface than in case of AM materials in spite of its lower hardness.
3. The resultant cutting forces are lower for AM materials than the standard titanium in spite of their higher hardness. The forces, in general, increase with the increase in feed per tooth and depth of cut.
4. The burr formation on the top of the down milling side is significant for AM materials as compared to standard titanium. There are little or no burrs found when machining standard titanium. The burr formation seems to relate to laser power used for AM materials.

## Acknowledgements

The authors thank Quad Cities Manufacturing Laboratory in Moline, IL for producing the specimens and Sarah Wolf from Northwestern University for machining and preparing the specimens.

## References

[1] Atwood, C. et al., 1998. Laser Engineered Net Shaping (LENS): A Tool for Direct Fabrication of Metal Parts. Proceedings of the International Congress on Applications of Lasers and Electro-Optics ’98, pp.1–7.
[2] Gibson, I., Rosen, D.W. and Stucker, B., 2015. Additive Manufacturing Technologies. Additive Manufacturing Technologies, pp.17–40.
[3] Hsu, F.C., Hung, T.P., 2016. Post-treatment process of additive manufacturing for intramedullary nails by ultrasonic vibration machining, abrasive flow machining, and electropolishing technology, 4M conference
[4] Ezugwu, E. O., Wang, Z. M., 1997. Titanium alloys and their machinability—a review. Journal of Materials Processing Technology, 68(3), 262–274.
[5] Veiga, C., Davim, J.P. and Loureiro, A.J.R., 2013. Review on machinability of titanium alloys: The process perspective. Reviews on Advanced Materials Science, 34(2), pp.148–164.
[6] Ulutan, D., Ozel, T., 2011, Machining induced surface integrity in titanium and nickel alloys: A review, International Journal of Machine Tools and Manufacture, 51/3:250–280
[7] M’Saoubi, R. et al., 2015. High performance cutting of advanced aerospace alloys and composite materials, CIRP Annals - Manufacturing Technology, 64, pp. 557–580
[8] Vazquez, E., Gomar, J., Ciurana, J. and Rodríguez, C. A., 2015. Analyzing effects of cooling and lubrication conditions in micromilling of Ti6Al4V. Journal of Cleaner Production, 87(C), 906–913.
[9] Singh, K. K., Kartik, V. and Singh, R., 2015. Modeling dynamic stability in high-speed micromilling of Ti-6Al-4V via velocity and chip load dependent cutting coefficients. International Journal of Machine Tools and Manufacture, 96, 56–66.
[10] Guo, P., Zou, B., Huang, C., Gao, H., 2017. Study on microstructure, mechanical properties and machinability of efficiently additive manufactured AISI 316L stainless steel by high-power direct laser deposition, Journal of Materials Processing Technology, Volume 240, Pages 12-22.
[11] Montevecchi, F. et al., 2016. Cutting Forces Analysis in Additive Manufactured AISI H13 Alloy. In Procedia CIRP. pp. 476–479.
[12] Tebaldo, V., Faga, M.G., 2017. Influence of the heat treatment on the microstructure and machinability of titanium aluminides produced by electron beam melting, Journal of Materials Processing Technology, Volume 244, Pages 289-303.
[13] Bruschi, S., Tristo, G., Rysava, Z., Bariani, P. F., Umbrello, D. and De Chiffre, L., 2016. Environmentally clean micromilling of electron beam melted Ti6Al4V. Journal of Cleaner Production, 133, 932–941.
[14] Rysava, Z. et al., 2016. Micro-drilling and Threading of the Ti6Al4V Titanium Alloy Produced through Additive Manufacturing. Procedia CIRP, 46, pp.583–586.

[15] Kobryn, P., Semiatin, S., 2003. Microstructure and texture evolution during solidification processing of Ti–6Al–4V. Journal of Materials Processing Technology, 135(2-3), pp.330–339.
[16] Brice, C.A. et al., 1999. Process Variable Effects on Laser Deposited Ti-6Al-4V. In Solid Freeform Fabrication. pp. 369–374
[17] Wolff, S., Lee, T., Faierson, E., Ehmann, K., and Jian Cao, 2016. Anisotropic Properties of Directed Energy Deposition (DED)-Processed Ti-6Al-4V. 44th SME North American Manufacturing Research Conference (NAMRC 44).
[18] Dutta, B. & Froes, F.H., 2014. Additive manufacturing of titanium alloys. Advanced Materials and Processes, 172(2), pp.18–23.
[19] Bagheri, A. Shamsaei, N., Thompson, S.M., 2015. Microstructure and Mechanical Properties of Ti-6Al-4V Parts Fabricated by Laser Engineered Net Shaping. ASME 2015 International Mechanical Engineering Congress and Exposition, Volume 2A: Advanced Manufacturing.
[20] Hashimura, M., Hassamontr, J. & Dornfeld, D.A., 1999. Effect of In-Plane Exit Angle and Rake Angles on Burr Height and Thickness in Face Milling Operation. Journal of Manufacturing Science and Engineering, 121(1), p.13.